The evolution and distribution of recycled oceanic crust in the Earth's mantle: Insight from geodynamic models

Jun Yan[a], Maxim D. Ballmer[b, a, c], and Paul J. Tackley[a]

[a] Institute of Geophysics, ETH Zurich, Zurich, Switzerland

[b] Department of Earth Sciences, University College London, London, United Kingdom

[c] Earth-Life Science Institute, Tokyo Institute of Technology, Tokyo, Japan

Corresponding author: Jun Yan (jun.yan@erdw.ethz.ch)

Highlights:

- Compositional mantle layering is robustly predicted despite whole-mantle convection.
- Basalt-enhanced reservoir forms in the MTZ, independent of mantle viscosity profile.
- Basalt fraction in the MTZ is laterally variable, ranging from ~30% to 50%.
- A layer beneath the MTZ displays significant (40%~80%) enrichment in harzburgite.
- The bulk-silicate Earth may be enriched in basalt relative to upper-mantle pyrolite.

Keywords: recycled oceanic crust, compositional mantle layering, chemical heterogeneity, mantle transition zone, thermochemical convection

Abstract

A better understanding of the Earth's compositional structure is needed to place the geochemical record of surface rocks into the context of Earth accretion and evolution. Cosmochemical constraints imply that lower-mantle rocks may be enriched in silica relative to upper-mantle pyrolite, whereas geophysical observations support whole-mantle convection and mixing. To resolve this discrepancy, it has been suggested that subducted mid-ocean ridge basalt (MORB) segregates from subducted harzburgite to accumulate in the mantle transition zone (MTZ) and/or the lower mantle. However, the key parameters that control basalt segregation and accumulation remain poorly constrained. Here, we use global-scale 2D thermochemical convection models to investigate the influence of mantle-viscosity profile, planetary-tectonic style and bulk composition on the evolution and distribution of mantle heterogeneity. Our models robustly predict that, for all cases with Earth-like tectonics, a basalt-enriched reservoir is formed in the MTZ, and a harzburgite-enriched reservoir is sustained at 660~800 km depth, despite ongoing whole-mantle circulation. The enhancement of basalt and harzburgite in and beneath the MTZ, respectively, are laterally variable, ranging from ~30% to 50% basalt fraction, and from ~40% to 80% harzburgite enrichment relative to pyrolite. Models also predict an accumulation of basalt near the core mantle boundary (CMB) as thermochemical piles, as well as moderate enhancement of most of the lower mantle by basalt. While the accumulation of basalt in the

MTZ does not strongly depend on the mantle-viscosity profile (explained by a balance between basalt delivery by plumes and removal by slabs at the given MTZ capacity), that of the lowermost mantle does: lower-mantle viscosity directly controls the efficiency of basalt segregation (and entrainment) near the CMB; upper-mantle viscosity has an indirect effect through controlling slab thickness. Finally, the composition of the bulk-silicate Earth may be shifted relative to that of upper-mantle pyrolite, if indeed significant reservoirs of basalt exist in the MTZ and lower mantle.

1. Introduction

Mantle convection and plate tectonics are fundamental processes that control the distribution and evolution of chemical heterogeneity in the Earth's interior. One of the main mechanisms for generating chemical heterogeneity is the subduction of slabs that consist of the products (basaltic oceanic crust) and residues (harzburgite) of mid-ocean ridge melting, along with a sediment cover, into the mantle. While ancient (or "primordial") heterogeneity that results from the accretion and differentiation of our planet may have been preserved somewhere in the mantle (Ballmer et al., 2017; Mukhopadhyay, 2012; Mundl et al., 2017), much of it is thought to be processed through mantle convection and near-surface melting (e.g., Rizo et al., 2013; Christensen & Hofmann, 1994). Accordingly, most of the present-day mantle is likely a

mechanical mixture of basaltic and harzburgitic materials (and their high-pressure polymorphs), consistent with geophysical and geochemical constraints (e.g., Hofmann, 1997; Xu et al., 2008). Mantle structure and differentiation is controlled by convective mixing and chemical segregation of any such heterogeneity during the long-term evolution of the Earth (Brandenburg & van Keken, 2007).

Both geochemical and geophysical observations demonstrate that Earth's mantle is heterogeneous from small to large scales (e.g., Stixrude & Lithgow-Bertelloni, 2012 and references therein). For example, a large number of small-scale seismic scatters have been observed in the upper to middle layers of the lower mantle (Kaneshima & Helffrich, 1999). These scatters have mostly been attributed to the subduction and stirring of basalt, as their elastic properties agree with the expected properties of high-pressure basalt that is juxtaposed to pyrolite (Rost et al., 2008). The scale-length of the detected seismic heterogeneities is typically on the order of 10 km, which is also consistent with the typical thickness of subducted crust (Bentham & Rost, 2014). Recently, mid-scale reflectors have also been observed in the shallow lower mantle, and related to fossil subduction (Waszek et al., 2018).

Large-scale heterogeneity in the Earth's mantle is also evident from seismic observations. For example, two large low-shear-velocity provinces (LLSVP), which are 1000s km wide and ~1000

km in vertical extent, have been imaged in the lowermost mantle, one beneath the Pacific and the other beneath Africa (e.g., Dziewonski et al., 2010). Sharp gradients in seismic wave speeds at their edges (Garnero et al., 2016), an anti-correlation between shear-wave and bulk-sound velocities (e.g., Koelemeijer et al., 2015) and intrinsically high densities (Ishii & Tromp, 1999) support a compositional origin of these domains. One of the end-member hypotheses proposed for the origin of these compositional anomalies (i.e., thermochemical piles) is that basalt largely segregates from harzburgite and subsequently accumulates in the deep mantle (Brandenburg & van Keken, 2007; Christensen & Hofmann, 1994; Nakagawa & Tackley, 2005). Alternatively, a mixture of basalt with ancient material (e.g., magma-ocean cumulates) has been proposed in terms of LLSVP composition (Ballmer et al., 2016; Tackley, 2012).

Apart from the chemical heterogeneity in the lower mantle, it has been suggested that the subducted basalt is separated from harzburgite and gravitationally trapped in the MTZ. Accordingly, segregation may sustain the formation in a basalt-enriched heterogeneous reservoir, which may have various geochemical and geophysical consequences (Anderson, 1979; Ringwood & Irifune, 1988). For example, it has been suggested that some plumes may rise from the basalt-enriched reservoir in the MTZ to feed hotspot volcanism (e.g., Allègre & Turcotte, 1985), or that the accumulation of basalt in the MTZ on the backside of subducted slabs may leave an imprint on the geoid (Karato, 1997). The formation of this basalt-enriched reservoir has

been related to the density profile of basalt relative to pyrolite (see Fig. 1), which involves a density crossover at the ringwoodite-bridgmanite phase transition at 660 km depth. While basalt is denser than the surrounding mantle in the upper mantle and MTZ, it is less dense at depths of 660~800 km (Hirose et al., 1999; Irifune & Ringwood, 1993).

Whether or not a basalt reservoir in the MTZ can be formed depends on the efficiency of segregation of basalt from harzburgite in the subducted slab either in the MTZ or above the CMB. Estimates based on analytical and simplified Newtonian sandwich models establish that rheology controls segregation of mantle materials, in general, and indicate that subducted slabs may be sufficiently weak for segregation of basalt from harzburgite, in particular (Karato, 1997; van Keken et al., 1996; Lee and Chen, 2007). Fully coupled numerical models of regional (Davies, 2008; Motoki & Ballmer, 2015; Ogawa, 2000) and global-scale mantle convection (Ballmer et al., 2015; Nakagawa & Buffett, 2005; Nakagawa et al., 2010) support that significant amounts of basalt can segregate from harzburgite and accumulate in the MTZ. However, the extent of basalt accumulation as a function of physical parameters remains is poorly constrained in all previous studies. Indeed, a systematic parameter study has not yet been performed to quantify basalt segregation and accumulation in the deep mantle and MTZ.

In this study, we use global-scale 2D thermochemical convection models to quantify effects of mantle rheology, plate tectonic style and bulk composition on the evolution and distribution of chemical heterogeneity in the mantle. In particular, we focus on the effects of radial mantle viscosity profiles on the segregation and accumulation of basalt. We scrutinize the delivery of basalt to the MTZ and lowermost mantle, and formation of harzburgite-enriched reservoir just beneath the MTZ. Finally, we quantify the characteristic residence timescales of materials in these reservoirs.

2. Methods

We use finite-volume mantle-convection code StagYY (Tackley, 2008) to solve the conservation equations of mass, momentum and energy in a two-dimensional spherical annulus geometry of a compressible infinite Prandtl number fluid. The numerical model domain is resolved by 1024 × 128 cells with a radial grid refinement of up to 2 times near to the surface and CMB (i.e., ~10 km grid spacing). Resolution tests demonstrate that our current number of cells is sufficient to model segregation and entrainment of mantle materials (see Suppl. Fig. S1 and Appendix in Tackley, 2011). In order to track composition, five million Lagrangian tracers (~30 tracers per cell) are distributed in the model domain. The models take phase transitions, partial melting, time-dependent internal and basal heating, pressure and temperature-dependence of viscosity, as well

as plastic rheology into account. Kinematic boundary conditions are free slip at the top and bottom.

As in previous studies (e.g., Nakagawa & Tackley, 2012), mantle materials are described as mechanical mixtures of subducted/recycled oceanic crust and subducted/recycled oceanic lithosphere. Hereafter, we refer to these rock types as "basalt" and "harzburgite", respectively. Basalt and harzburgite and their respective high-pressure polymorphs are the end-members of our one-dimensional compositional parameterization (see below). They represent any mafic and ultramafic lithology, respectively, that has a similar density profile and melting behavior as modeled here (e.g., Fig. 1). In this parameterization, pyrolitic mantle corresponds to a mechanical mixture of ~20% basalt and ~80% harzburgite (Xu et al., 2008). End-members basalt and harzburgite are defined as a solid solution of olivine (ol) and pyroxene-garnet (px-gt) mineral systems (harzburgite: 75% ol and 25% px-gt; basalt: 100% px-gt). Each of these systems is parameterized to undergo the relevant solid-state phase transitions (see Suppl. Table S1). The density profiles of mantle materials are then calculated from our parameterization of major phase transitions, and the thermodynamic parameters of each phase. These density profiles, as shown in Figure 1, are consistent with those derived by Xu et al. (2008).

We apply a strongly temperature and pressure-dependent rheology using an Arrhenius-type formulation:

$$\eta_{viscous}(T,p) = \prod_{ij} \lambda_{ij}^{f_j \Gamma_{ij}} \eta_0 \exp\left(\frac{E+pV}{RT} - \frac{E}{RT_0}\right) \quad (1)$$

where η_0 and T_0 are the reference viscosity and reference temperature (i.e., at the surface at zero pressure), respectively; E is activation energy; p is pressure; V is activation volume; T is absolute temperature, and R the ideal gas constant; Viscosity jumps are imposed at the phase transitions as suggested by mineral physics experiments and theoretical calculations (e.g., Ammann et al., 2010). λ_{ij} is the viscosity jump caused by phase transition (i, j) (see Suppl. Table S1), f_j is the fraction of phase system j (olivine or pyroxene-garnet), Γ_{ij} is the phase function for each phase (Nakagawa & Tackley, 2010). The relevant viscosities in each mantle layer are free model parameters in this study (see below).

In order to obtain plate-like tectonic behavior, plastic yielding is included using a Drucker-Prager yield criterion with a pressure-dependent effective yield-stress parameterization:

$$\eta_{yield} = \frac{C+p\mu}{2\varepsilon_{II}} \quad (2)$$

where μ is the friction coefficient, C the cohesion coefficient and ε_{II} the second invariant of the strain rate tensor. The effective viscosity is defined by the minimum of the two components from equation (1) and (2):

$$\eta_{eff} = min(\eta_{viscous}, \eta_{yield}) \quad (3)$$

Partial melting generates basaltic oceanic crust and a complementary depleted residue. At each time step, the temperature in each cell is compared to the solidus temperature. As long as the temperature in a specific cell exceeds the solidus, melt is generated to bring the temperature back to solidus, leaving a residue behind with a depletion that depends on the related degree of melting. For details, see Nakagawa & Tackley (2010) and references therein.

The initial condition for temperature is an adiabatic temperature profile with a potential temperature of 2000 K with thermal boundary layers at the top and bottom of the model box. The surface temperature is set at 300 K. The initial CMB temperature is assumed to be 5913 K. The core cools as heat is extracted by the mantle as in Nakagawa & Tackley (2010). Internal heating is also time-dependent, initially being H_r and decaying according to a timescale τ, which is similar to the characteristic half-life of the dominant heat-producing radionuclides in the Earth's mantle. Our models are initialized with homogeneous composition, i.e., in most cases with pyrolitic composition, which corresponds to a mechanical mixture of 20% basalt and 80% harzburgite in most of our models.

All physical parameters used in the model are listed in the Suppl. Table S2. Hereinafter, we refer to basalt fraction (compositional index) as X_{BS}. This simplified compositional index is a

169 projection of multi-oxide mantle rock composition on one single axis, and defined to range from
170 0 (harzburgite) to 1 (basalt), with pyrolite being ~0.2.

171 **3. Results**

172 ***3.1. Model predictions for the reference case***

173 Before exploring the parameter sensitivity of our models, we first describe in detail the
174 distribution and evolution of chemical heterogeneity in our reference model (for initial
175 temperature and viscosity profiles, see Suppl. Fig. S2-3). The reference case is characterized by a
176 viscosity jump of a factor 30 at 660 km depth, but no viscosity jump at 410 km depth (for other
177 relevant parameters, see Suppl. Table S2). Due to our visco-plastic rheology, slabs of basalt and
178 harzburgite are continuously introduced into the mantle at various subduction zones over 4.5 Gyr
179 model time.

180 Despite whole-mantle convection, compositional layering is predicted to occur across the mantle
181 over large regions (Fig. 2). A basalt-enriched reservoir is commonly formed over large regions at
182 the base of the MTZ (i.e., just above 660 km depth), and a complementary harzburgite-enriched
183 reservoir is formed just below 660 km depth. In addition, large-scale heterogeneous
184 thermochemical piles accumulate at the base of the mantle. On top of these strongly-enhanced
185 reservoirs visible in Figure 2, the average radial profile of basalt fraction X_{BS} (Fig. 3a) shows that

186 the composition of the uppermost mantle is generally shifted toward harzburgite, while most of
187 the lower mantle is relatively enhanced in basalt (see section 3.4). The formation of this global
188 compositional layering in the presence of mantle convection requires segregation of basaltic
189 materials from depleted harzburgitic, and is ultimately controlled by the density profiles in
190 Figure 1. In general, compositional segregation competes with convective stirring (i.e.,
191 mechanical mixing) in the convecting mantle.

192 Figure 3b shows that the mantle geotherm of the reference case is generally subadiabatic.
193 Subadiabatic geotherms are typical for whole-mantle convection models (Sinha & Butler, 2007),
194 in which plumes rise to feed the uppermost mantle, and slabs sink to the base of the mantle (Fig.
195 2f). On top of a generally subadiabatic geotherm, there are potential-temperature minima and
196 maxima in and just below the MTZ, respectively, over most of mantle evolution. We attribute
197 these minima and maxima to slabs that stagnate at 660 km depth, and warm harzburgite that
198 accumulates just beneath, respectively. We also note that the predicted mantle temperatures are
199 ~200 K higher than realistic, which may be due to the distribution of internal heat sources (see
200 Suppl. Fig. S4).

201 Segregation of mantle rock types and the related large-scale layering of small-scale heterogeneity
202 are promoted by the density difference between harzburgitic and basaltic materials as a function

of depth (Fig. 1). Models predict that the first segregation of basalt from harzburgite (i.e., within the subducted slab) usually occurs in the hot thermal boundary layer near the CMB, where the viscosity is lowest (also see Karato, 1997; Tackley, 2011). Note that decreasing viscosities tends to promote segregation of short-length heterogeneity as the growth rate and wavelength of Rayleigh-Taylor instability is reduced. Subsequently, larger blobs of basalt are transported by mantle convection (e.g., plumes), and ultimately accumulate in a given layer based on the well-constrained density profile in Figure 1. Basalt is denser than pyrolite and harzburgite through most of the mantle, and hence tends to accumulate in the lowermost mantle. In turn, harzburgite tends to accumulate in the upper mantle. Accumulation of basalt in the MTZ is explained by the density crossover that occurs at the base of the MTZ (there is no such accumulation in a test case without density crossover; see Fig. 3c-d). Since basaltic materials are less dense than the surrounding mantle at depths of 660-720 km (Fig. 1), they tend to be gravitationally trapped in the MTZ. Conversely, harzburgitic materials tend to be trapped just below the MTZ (see arrows in Fig. 1).

In more detail, our reference model predicts that deep-rooted plumes as well as stagnant slabs transport basalt to the MTZ in order to establish the basalt-enriched reservoir. At early model times <~0.5 Gyr, subducted slabs play the major role in transporting basalt to the MTZ. Due to the viscosity and density jump at the ringwoodite-to-perovskite phase transition (i.e., coupled

221 with its negative Clapeyron slope) at 660 km depth, the cold and strong slabs stagnate in the
222 MTZ and subsequently become warm and weak as they are heated. This heating promotes the
223 segregation of basalt from harzburgite (Motoki & Ballmer, 2015), in this case directly in the
224 MTZ. Apart from stagnant slabs in the MTZ, many subducted slabs penetrate through the MTZ
225 and sink into the deep mantle. As they reach the deep mantle, basaltic components segregate
226 from harzburgite near the CMB, and subsequently accumulate above the CMB, forming the first
227 basalt-enriched thermochemical piles (Fig. 2a-b), which subsequently grow (Fig. 2c). At later
228 model times (i.e., > ~0.5 Gyr), the mantle lithosphere becomes stronger as the mantle (and core)
229 progressively cool(s). This strengthening tends to make subduction less efficient, resulting in
230 slower plate speeds, fewer subduction zones, and larger plate thicknesses. In this phase, basalt is
231 most efficiently delivered by plumes to MTZ due to entrainment from thermochemical piles.
232 Chunks of basalt are "lost" by plumes to accumulate in the MTZ, because of its large density
233 anomaly (Fig. 1) as well as the relatively low viscosity in the MTZ.

234 In addition to the transport of basalt to the MTZ by plumes (and slabs), the balance of basalt in
235 the MTZ is controlled by processes for basalt removal. Episodic removal of basalt from the MTZ
236 is accomplished by three mechanisms. First, downgoing subducted slabs can entrain materials
237 that accumulate in or at the base of the MTZ, thus potentially "cleaning out" any regional basalt-
238 enriched reservoir (along with the underlying harzburgite-enriched reservoir). This mechanism is

239 dominant among the three mechanisms, especially at relatively late model times (> ~0.5 Gyr).
240 Second, large mantle plumes can likewise entrain (or push out) any layered material from (the
241 base of) the MTZ. Third, as the basalt-enriched layer grows beyond a critical thickness, it
242 becomes gravitationally unstable and promotes diapiric basaltic avalanches (encircled by white
243 ellipses in Fig. 2d-e). Nevertheless, as basalt is continuously delivered to the MTZ, regional
244 reservoirs can be sustained for long model times, and e.g., just be swept laterally, mostly
245 maintaining isostatic equilibrium. Hence, the global basalt profile soon reaches (after ~0.5 Gyrs)
246 and maintains a statistical steady state (Fig. 3a).

247 To quantify the distribution of heterogeneity in the mantle, Figure 4a-b shows histograms of
248 average X_{BS} (and corresponding basalt and harzburgite enrichment) in layers just above and just
249 below 660 km from 2 to 4.5 Gyr. Just above 660 km depth, X_{BS} is widely 30%~50%,
250 corresponding to basalt enrichments (relative to pyrolite) of 12%~37% (Fig. 4a). However, there
251 are also some strongly-enriched ($X_{BS} >> 50\%$) and pyrolitic ($X_{BS} \approx 20\%$) regions. In turn, the
252 dominant volume of the layer just below 660 km depth displays $X_{BS} \approx 10\%$, corresponding to
253 harzburgite enrichments of 40%~80%. Fig. 4c shows that the volume of basalt-enriched piles
254 remains nearly constant over the last 2.5 Gyr.

Finally, Figure 4d-f shows the distributions of basalt/harzburgite ages for the relevant reservoirs in/beneath the MTZ and above the CMB. The dominant basalt and harzburgite ages in both basalt-enriched and harzburgite-enriched reservoir are ~2 Gyr. This can be seen as a rough timescale for the delivery of materials to plus their residence time in these reservoirs. Only small volumes of the basalt-enriched reservoir are younger than 1 Gyr, which is an indicator of the minor role of delivery by young subducted slabs. In turn, the basalt-age distribution across the depth range of 2390-2890 km is bimodal (Fig. 4f): young subducted basalt (<1 Gyr) with dominant ages of ~0.5 Gyr and old subducted basalt (> 2 Gyr) with dominant ages of ~2.5 Gyr (the latter mostly comprising thermochemical piles). That basalt-enriched piles can survive for billions of years is consistent with previous work (e.g., Mulyukova et al., 2015). Note that the harzburgite reservoir in the uppermost lower mantle also displays a bimodal distribution (Fig. 4e), but the basalt reservoir in the MTZ does not (Fig. 4d). This result highlights the segregation of basalt from harzburgite in the lower mantle. Whereas both young and old harzburgite can be delivered to the reservoir beneath the MTZ due to its intrinsic buoyancy, only old basalt is delivered to the MTZ. Before delivery, basalt is stored in thermochemical piles to be heated and overcome its intrinsic density anomaly, and eventually be entrained by plumes.

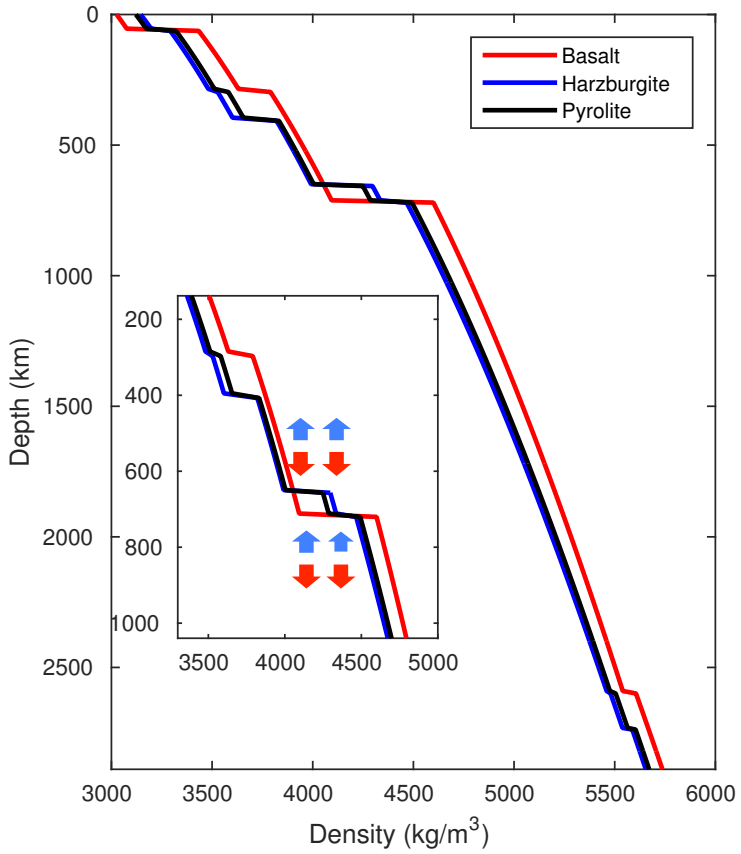

271

272 **Fig. 1.** Density profiles for basalt (100% pyroxene-garnet), harzburgite (75% olivine + 25%

273 pyroxene-garnet) and pyrolite (20% basalt + 80% harzburgite). Note the density crossover

274 between 660 and 720 km. We parameterize the gradual breakdown of garnet (Hirose et al., 1999;

275 Irifune & Ringwood, 1993) as a transition of width 75 km (see Suppl. Table S1) at 720 km depth.

276 The red and blue arrows denote the negative and positive buoyancy of basalt and harzburgite

277 away from this crossover region, respectively.

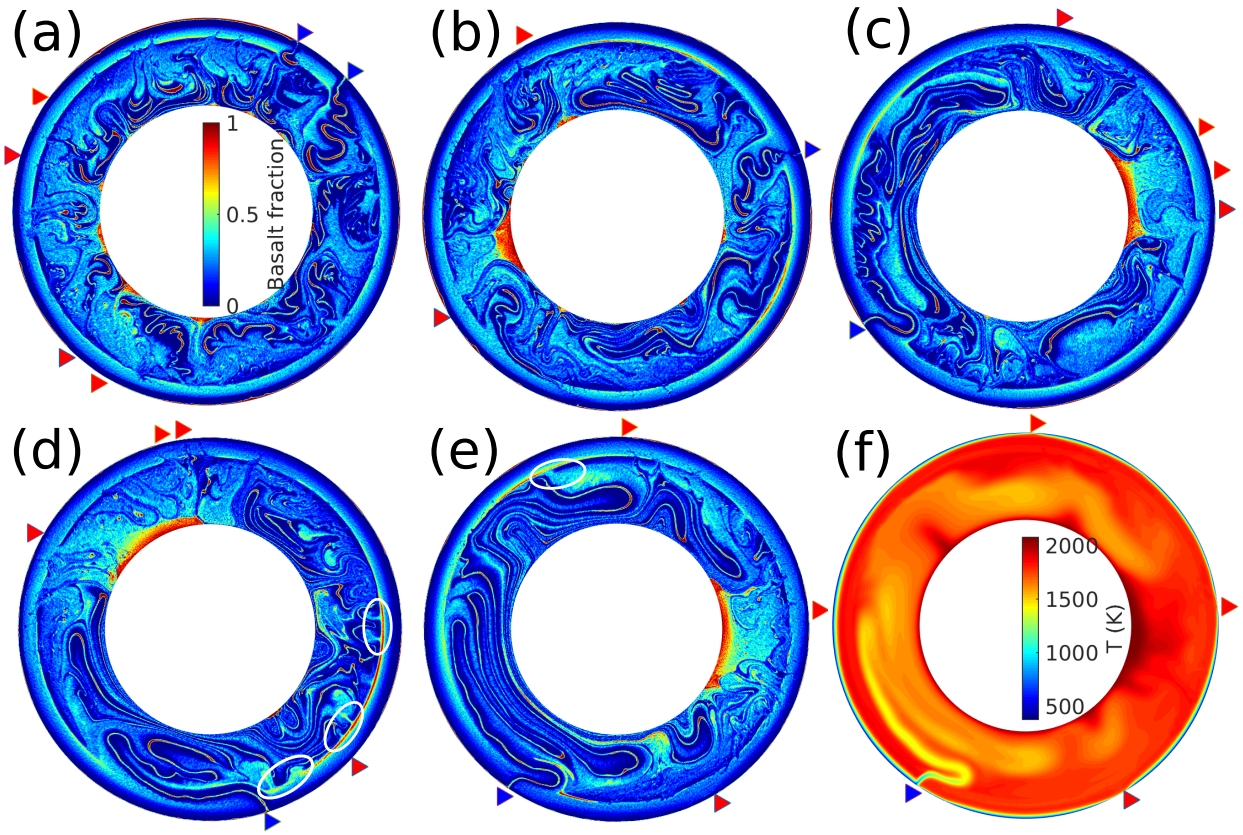

278

279 **Fig. 2.** Snapshots of X_{BS} (compositional index) at model times (a) 1.0 Gyr (b) 2.0 Gyr (c) 3.0 Gyr

280 (d) 4.0 Gyr (e) 4.5 Gyr; (f) potential temperature T at 4.5 Gyr for the reference model. Blue and

281 red triangles refer to subduction zones and mid-ocean ridges, respectively. White ellipses denote

282 the diapiric basaltic avalanches. Rising plumes are readily identified in panel (f). For movies of

283 the compositional and thermal evolution of the reference case, we refer the reader to the

284 supporting online information (Suppl. Movie S1).

285

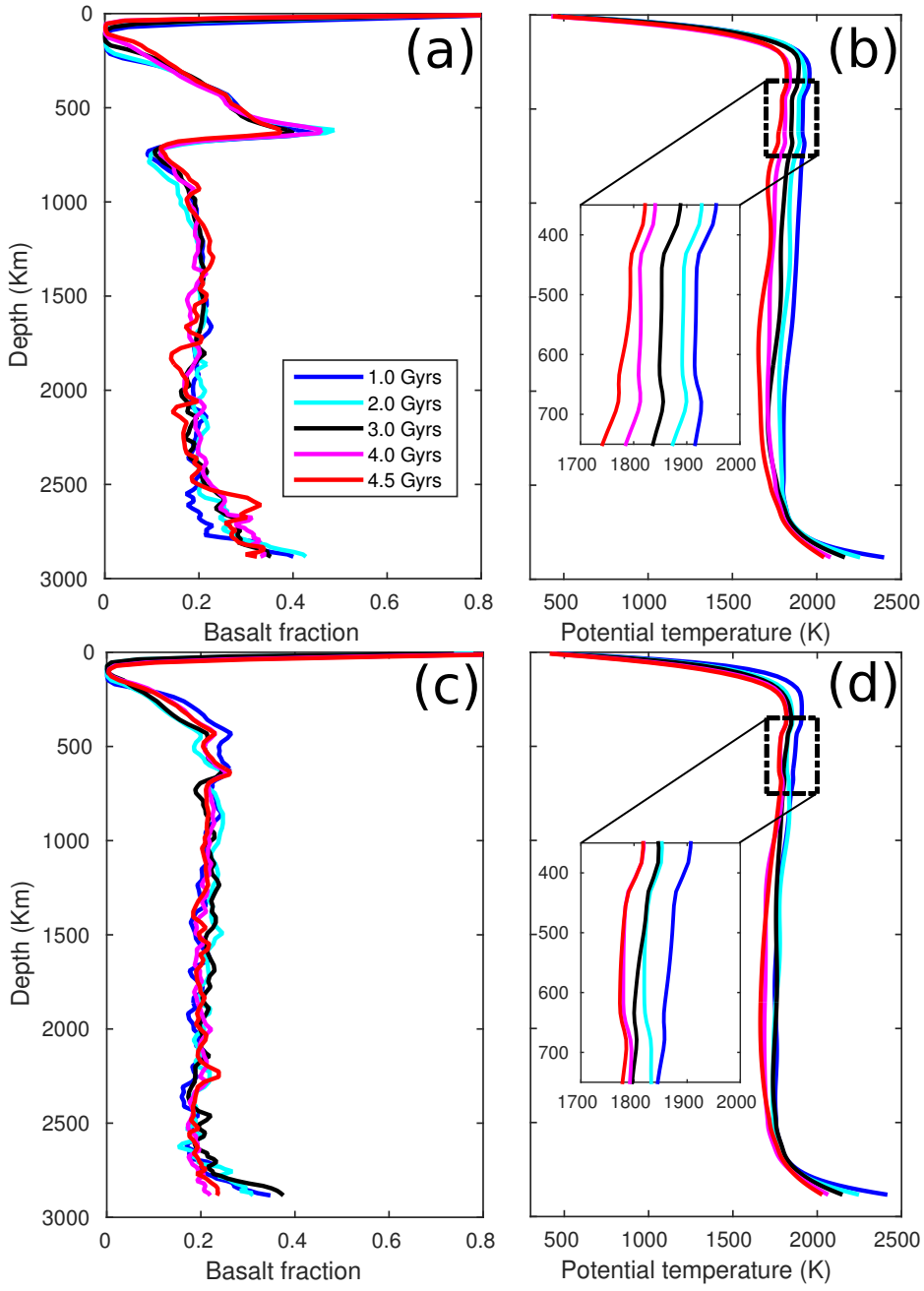

Fig. 3. Radial average profiles of (a) X_{BS} (compositional index) and (b) potential temperature for the reference case at different model times (from 1.0 to 4.5 Gyr as labeled). For comparison, (c) X_{BS} (compositional index) and (d) potential temperature for a test case, in which the density crossover at 660-720 km depth is artificially switched off (i.e., the depth of the phase change in

291 the px-gt system is set to 660 km instead of 720 km). In this test case (with otherwise the same
292 parameters as for the reference model), no basalt-/harzburgite-enriched reservoir is formed just
293 above/beneath 660 km. Note detailed potential-temperature gradients across the MTZ as shown
294 in insets.
295

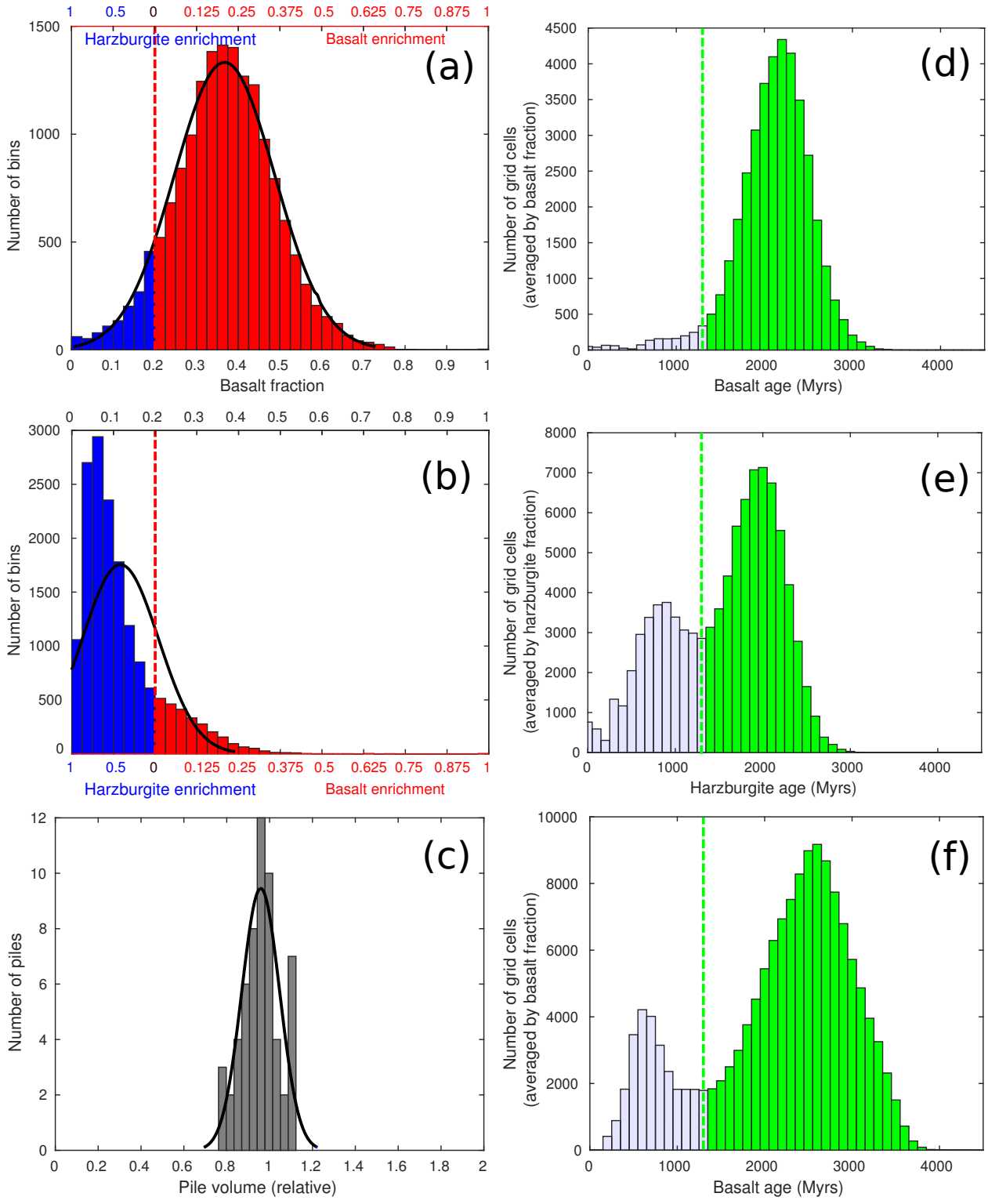
(a)
Harzburgite enrichment
Basalt enrichment
Number of bins
Basalt fraction
(b)
Harzburgite enrichment
Basalt enrichment
Number of bins
(c)
Number of piles
Pile volume (relative)
(d)
Number of grid cells
(averaged by basalt fraction)
Basalt age (Myrs)
(e)
Number of grid cells
(averaged by harzburgite fraction)
Harzburgite age (Myrs)
(f)
Number of grid cells
(averaged by basalt fraction)
Basalt age (Myrs)

296

297

298 **Fig. 4.** Distribution of heterogeneity (i.e., in terms of X_{BS}, basalt age and relative volume) in the
299 MTZ (i.e., at depths of 560-660 km, a and d), just beneath the MTZ (i.e., at depths of 660-760
300 km, b and e), and above the CMB (i.e., at depths of 2390-2890km, c and f). Note that the black
301 curve in each histogram is the corresponding normal distribution, plotted for reference. Red and
302 green vertical lines denote the boundaries between basalt enrichment and harzburgite enrichment,
303 and between relatively young and old reservoirs, respectively. For each bin (~3 degrees wide) in
304 panels (a-b), composition is averaged over the depth range labeled. Bins are summed into
305 histograms over model times 2-4.5 Gyr, scaled by (a) X_{BS}, or (b) 1-X_{BS}. In (c), pile volumes are
306 measured over 2-4.5 Gyr, and normaliized by that in the last time-step of the reference case
307 (Figure 2e). In (e-f), basalt ages at grid cells are summed into histograms over 3.5-4.5 Gyr.

308

309 ***3.2. Effects of mantle viscosity***

310 To investigate the influence of mantle viscosity on the segregation and accumulation of basalt in
311 the mantle, we systematically vary three model parameters: (1) the viscosity jump due to the
312 phase change at 410 km; (2) the viscosity jump due to the phase change at 660 km; and (3) the
313 reference viscosity. Combining these three parameters, we generate four groups of radial mantle
314 viscosity profiles (see Suppl. Fig. S3). In each of these four groups, the viscosities are varied by

315 up to a factor of ~100 in (A) the uppermost mantle (i.e., at depths <410 km), (B) the MTZ (i.e.,
316 at depths of 410-660 km), and (C) the lower mantle (i.e., at depths >660 km), and (D) the whole
317 mantle, respectively.

318 In group A, our results suggest that relatively high uppermost-mantle (plus lithospheric)
319 viscosities have no or little effects on the accumulation of basalt in the MTZ (Fig. 6a), while they
320 tend to result in larger harzburgite-enriched reservoir beneath the MTZ and higher amounts of
321 basalt above CMB (see e.g., Figs. 5a, 6e and 6j). Models show that relatively high uppermost-
322 mantle viscosities are associated with thicker plates and larger crustal thicknesses (see Suppl.
323 Figs. S7a and S8a). The related thicker subducted slabs promote segregation of basalt from
324 harzburgite in the lower mantle, ultimately leading to larger amounts of harzburgite just beneath
325 the MTZ (Fig. 6e) and larger basalt-enriched piles above the CMB (Fig. 6j). Besides, thicker
326 plates also result in slower plate velocities (i.e. root-mean-square velocity at the surface) and
327 lower plate mobilities (see Suppl. Figs. S5a and S5e), hence inhibiting mantle and core cooling
328 (see Suppl. Figs. S6a and S6e), thereby promoting partial melting, resulting in a more depleted
329 uppermost mantle (i.e., less X_{BS} in Fig. 5a). In turn, relatively low uppermost-mantle viscosities
330 are associated with thinner plates. While segregation of thinner subducted slabs is inefficient in
331 the deep mantle; this is not the case in the upper mantle and MTZ. Thinner slabs tend to stagnate
332 more readily in the MTZ since they are relatively weak, and segregate there into their basaltic

and harzburgitic components as they are warmed up. This effect trades off with the negative effect of slab (or subducted crustal) thicknesses on segregation in the lower mantle. Therefore, uppermost-mantle viscosities do not have obvious effects on the amount of basalt-enriched reservoir in the MTZ.

In group B, our models show that the X_{BS} in the MTZ is systematically controlled by MTZ viscosity (see Figs. 5b and 6b). However, this control is not very strong: the final average X_{BS} in the MTZ ranges between 30% and 37% in all cases of Group B (Fig. 5b). Besides, we find that relatively low viscosities in the MTZ (and a related large viscosity jump at the 660 km) tend to increase the resistance of the mantle to slab sinking, which leads to a relatively large amount of basalt accumulated in the MTZ from 1 to 2 Gyr. For relatively high viscosities in the MTZ, models predict instead that X_{BS} in the MTZ is relatively low throughout the entire history of mantle evolution. The variation of viscosities in the MTZ has little or no effects on the volume of basalt piles that accumulate above the CMB (Fig. 6k), or on the harzburgite-enriched reservoir just beneath the MTZ (Fig. 6f). An exception is that the volume of piles is somewhat increased for very low MTZ viscosities (such as case B1), as the efficiently segregated basalt in the MTZ ultimately reaches the CMB.

In group C, our models predict that the harzburgite-enrichment beneath the MTZ (Fig. 6g) as well as the volume of basalt-enriched piles above the CMB (Fig. 6l) increase with decreasing lower-mantle viscosity. This result is well explained by the effects of mantle viscosity on the efficiency of segregation. Any harzburgite segregated in the lower mantle tends to rise and eventually accumulate just below 660 km depth, and any segregated basalt tends to sink and eventually accumulate above the CMB. In turn, X_{BS} in the MTZ is largely independent of (i.e., only very slightly increases with) lower-mantle viscosity (see Figs. 5c and 6c). We attribute this result to a trade-off: while inhibiting segregation of basalt in the deep, higher lower-mantle viscosities tend to stabilize the conduits between convection cells, which facilitates the entrainment of basalt through these conduits (see Suppl. Movie S2-3). Moreover, higher lower-mantle viscosities tend to promote slab stagnation in the MTZ by increasing the viscosity jump at the 660. In combination, these two effects result in a slightly stronger enhancement of basalt in the MTZ (Fig. 5c, case C4), which confirms that both slabs (from above) and plumes (from below) deliver basalt to the MTZ.

In group D, we find that relatively low whole-mantle viscosities tend to enhance the segregation of basalt from harzburgite, promoting the enhancement of basalt in the MTZ (Fig. 6d) and deep mantle (Fig. 6m), as well as that of harzburgite just beneath the MTZ (Fig. 5d, 6h). This result can be explained by the combination of all effects discussed above. For example, for relatively

low whole-mantle viscosities, enhancement of basalt in the MTZ already occurs at early model times, and remains rather stable over billions of years with small second-order variations (see Suppl. Movie S1 and S4). These variations reflect the partial destruction of any basalt-enhanced layer in the MTZ (e.g., by sinking slabs), and subsequent replenishment. Similar to group C, lower whole-mantle viscosities promote segregation in the deep mantle to sustain large piles (see Fig. 6m). The formed piles are able to survive for several billions of years as any entrainment is usually (over)compensated by continued addition of basalt through segregation.

Despite the aforementioned variations, we stress that the predicted basalt contents (i.e., X_{BS}) in the MTZ are fairly robust over a wide range of viscosity profiles. While relatively low local mantle viscosity can promote the segregation and accumulation of basalt in the MTZ, average X_{BS} in the MTZ range from 0.3 to 0.35 (i.e., corresponding to 12.5%–18.7% basalt enrichment) for most cases, and up to 0.4 only for a few cases (see Figs. 6a-d). While for some cases (A4 and D4), the predicted average X_{BS} are < 0.3, these cases are not Earth-like, because of very small CMB heat fluxes and plate velocities (see Suppl. Figs. S5-6).

Similarly, the average harzburgite content (i.e., $1–X_{BS}$) in the thin layer just below 660 km depth is mostly parameter-independent. It is just sensitive to the viscosity in the lower mantle, as is explored in groups C and D. Furthermore, it slightly varies with parameters that control slab

384 thickness, such as uppermost-mantle viscosity. Nevertheless, the average harzburgite enrichment
385 at 660-760 km depth of most cases (except cases that are not Earth-like as mentioned above) just
386 varies between 25% to 50%, which corresponds to with 10% < X_{BS} < 15% (Figs. 6e-h).

387 In turn, the volume of piles above the CMB is strongly sensitive to the mantle viscosity profile
388 (Figs. 6j-m). Some cases result in no piles at all while other cases lead to very large pile volumes
389 that are about twice as large as in the reference case (see Fig. 2e). This result is well explained by
390 a variable balance between segregation and entrainment across cases in the context of a quasi-
391 infinite capacity of the deep-mantle reservoir (i.e., little or no feedback between pile volumes
392 and entrainment). The efficiency of segregation is controlled by the local (i.e., lower-mantle)
393 viscosity, and the thickness of the delivered basaltic slabs.

394 Overall, two processes occur in the mantle: segregation and accumulation. Segregation of basalt
395 from harzburgite is a prerequisite for the subsequent accumulation of basalt in/near the
396 MTZ/CMB (or of harzburgite just below the MTZ). Our models suggest that the balance
397 between delivery and removal controls the content of basalt/harzburgite in various mantle
398 reservoirs. Delivery and removal are controlled by the scale-length of heterogeneity and the local
399 viscosity, and thereby parameter-dependent. That the basalt content in the MTZ is robust over a
400 wide range of parameters is explained by the variety of processes that deliver basalt to the MTZ

401 (mostly plumes, but also stagnant slabs), and remove basalt from the MTZ (mostly sinking
402 slabs). These processes do not depend on the same parameters. Importantly, any process for
403 removal becomes more efficient as the MTZ is more enriched in basalt. Thus, the MTZ basalt
404 contents are ultimately controlled by its capacity. In contrast, the harzburgite layer just below
405 660 km depth gets mostly replenished by just one process (i.e., harzburgite rising through the
406 lower mantle), the efficiency of which depends on various parameters, mostly lower-mantle
407 viscosity (see above). We highlight that our models robustly predict that the MTZ is enriched in
408 basalt, and constrain the typical degree of enrichment as ~15% relative to pyrolite (i.e., $0.3 < X_{BS}$
409 < 0.35). All models display a subadiabatic potential-temperature gradient across the MTZ.

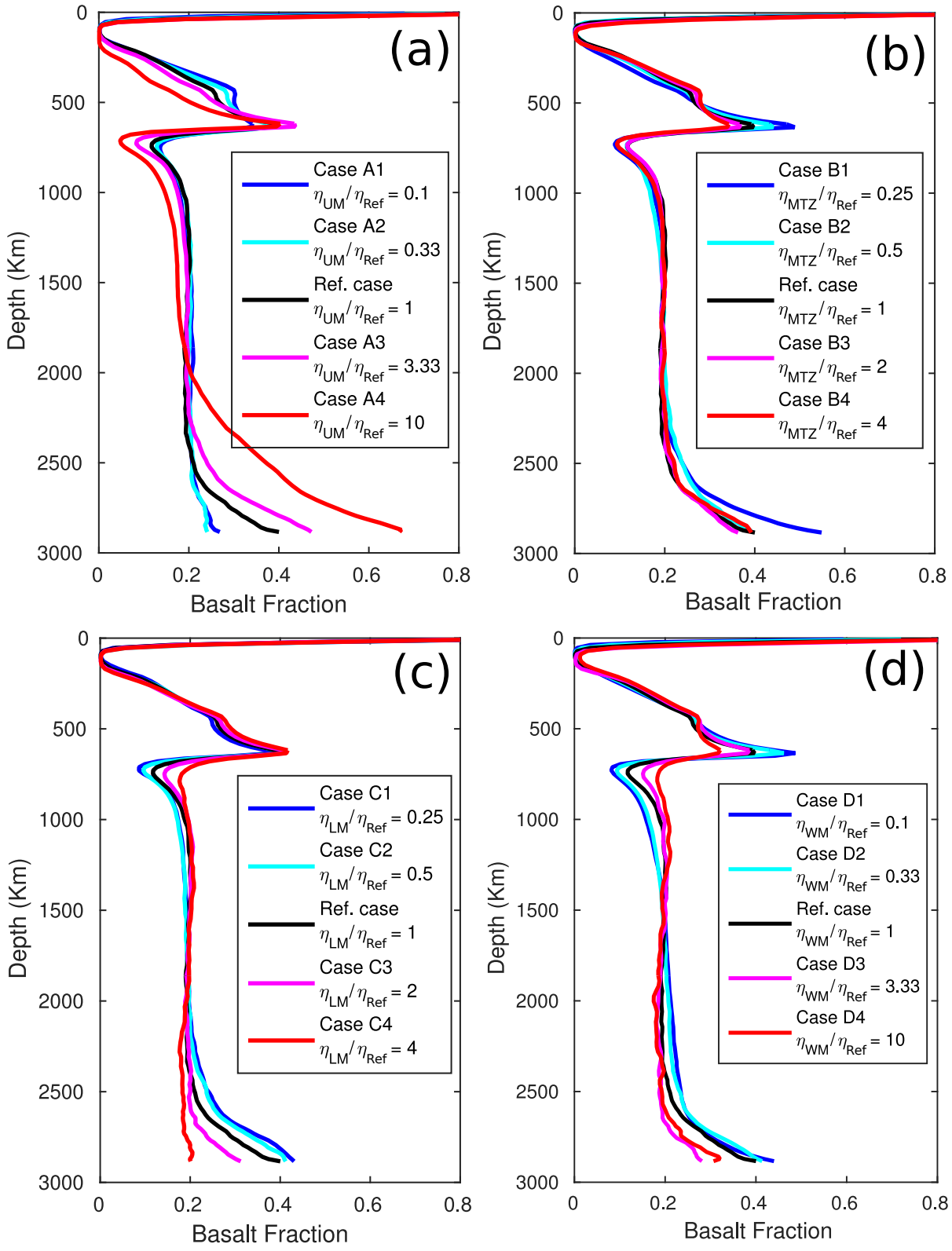

410

411 **Fig. 5.** Radial profiles of X_{BS} (compositional index), averaged laterally and over time (i.e.,

412 between 2 and 4.5 Gyr) for (a) group A: the uppermost-mantle (UM) viscosity (b) group B: MTZ

viscosity (c) group C: the lower-mantle (LM) viscosity (d) group D: the whole-mantle (WH) viscosity. Note that η_{UM}, η_{MTZ}, η_{LM} and η_{WM} denote uppermost-mantle viscosity, MTZ viscosity, lower-mantle viscosity, and whole-mantle viscosity, respectively. Correspondingly, η_{Ref} denotes the viscosity of the reference case.

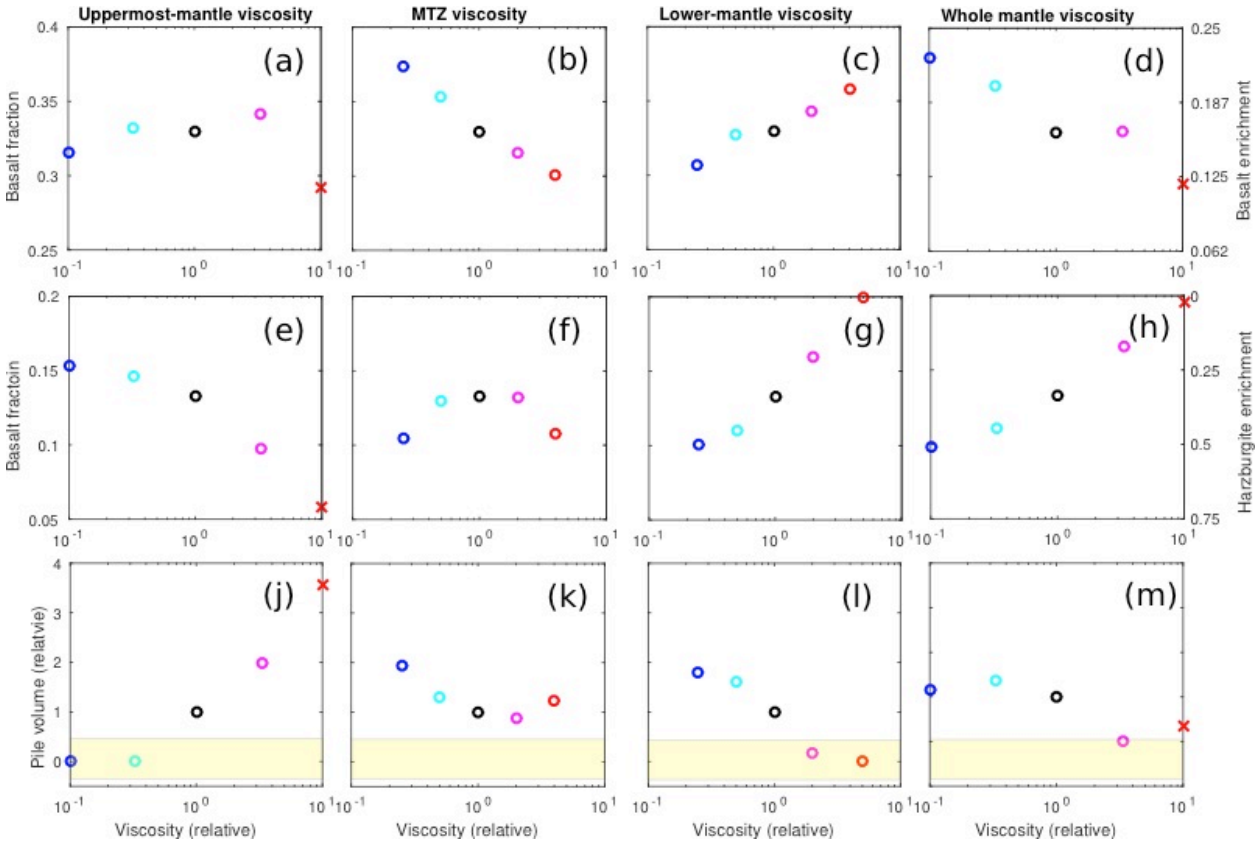

Fig. 6. Parameter sensitivity of the predicted composition of mantle layers. (Top row) Basalt fraction X_{BS} (compositional index), and corresponding basalt enrichment relative to pyrolite in the MTZ (i.e., at depths of 560-660 km), averaged laterally and over time (i.e., from 2 to 4.5 Gyr) for all cases in groups A-D (from left to right columns). (Middle row) X_{BS} and corresponding harzburgite enrichment just beneath the MTZ (i.e., at depths of 660-760 km) for all cases in

groups A-D. (Bottom row) relative volume (i.e., relative to the pile volume of the reference case at 4.5 Gyr (see Fig. 2e)) of basalt-enriched thermochemical piles (i.e., the threshold value of X_{BS} > 30% is used to discriminate piles and ambient mantle composition) above the CMB (i.e., at depths of 2590-2890 km). Crosses denote cases that do not match our criteria for Earth-like tectonic style (see Suppl. Fig. S5-6). The light yellow area shows cases with very small or no piles. For colors, see Fig. 5 legend.

3.3. Effects of plate-tectonic style

Next, we investigate the effects of an important but poorly constrained parameter for tectonic behavior of planets: the effective yield stress. While relatively low values sustain plate-tectonic behavior, large values promote the formation of a stagnant lid (e.g., Nakagawa & Tackley, 2015). We vary the effective yield stress by systematically changing the friction coefficient μ between 0.005 and 0.08 (see eq. 2 and 3). As we explore the effective yield stress, we keep all other parameters, including the viscosity profile, fixed.

We find that the activity of tectonics systematically varies within the relatively narrow range of friction coefficients μ explored here. For example, for the case E4 with the highest μ = 0.08, plate tectonics remains episodic with intermittent episodes of stagnant-lid tectonics (i.e., plate

441 mobility is episodically zero). All other cases display persistent plate tectonics. We find that the
442 number of subduction zones and, plate mobility, and average speed of tectonic plates increase
443 with decreasing yield stress (Fig. 7a). Therefore, more slab material is conveyed into the mantle
444 for small yield stresses, promoting planetary cooling, and ultimately reducing the extents of
445 basalt melting (see Fig. 7c where case E1 and E2 are featured with less depleted upper mantle).
446 Accordingly, crustal thicknesses are smaller for lower yield stresses. The related more active
447 subduction and sinking of (thinner) slabs continuously cleans out the MTZ through time such
448 that for case E1 stable basalt-enriched reservoir in the MTZ cannot be established at all (Fig. 7b).
449 Slab thicknesses and crustal thicknesses also have a strong effect on the segregation of
450 heterogeneity in the lower mantle. Similar to results in group A, higher yield stresses associated
451 with thicker subducted slabs result in larger basalt-enriched piles above the CMB (Fig. 7c).
452 Another effect involves the influence of planetary cooling as a function of yield stress on mantle
453 viscosity, and thereby on the distribution of heterogeneity (i.e., again in analogy to group A
454 above). Finally, it should be noted that there is a visible accumulation of basalt in the MTZ,
455 delaminated from the base of the crust in a stagnant lid regime (Armann & Tackley, 2012;
456 Nakagawa & Tackley, 2015) with high yield stress. That all said, we stress that neither relatively
457 low (case E1) nor high (case E4) yield stresses are relevant for the Earth. This further confirms
458 that the yield stress used in our reference case (and all other cases in groups A-D and F) is

reasonable for generating Earth-like plate tectonics, although there remains uncertainty in terms of this parameter.

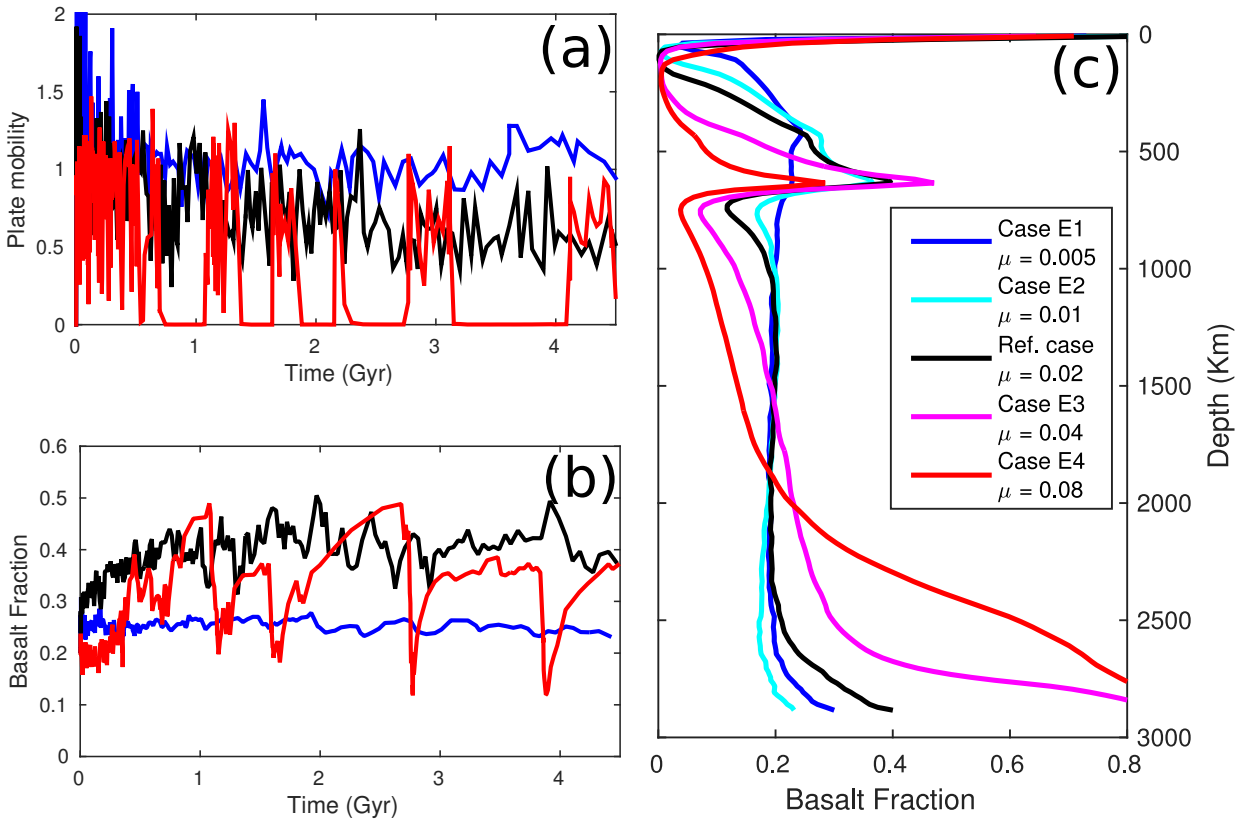

Fig. 7. (a) Plate mobility, (b) radial average X_{BS} (compositional index) in the MTZ form 0 to 4.5 Gyr, and (c) radial average X_{BS} (compositional index) between 2 and 4.5 Gyr for cases with the different friction coefficient μ.

3.4. Effects of initial mantle composition

Finally, we investigate the influence of initial mantle composition on the distribution of heterogeneity in the mantle. We vary the initial X_{BS} of the mantle, from 0.25 to 0.4. Thereby, the bulk composition of the silicate Earth is shifted towards that of basalt. In general, it is accepted that the source of MORB melting (i.e., the uppermost mantle) consists of pyrolite, which is similar to the rock type peridotite (Ringwood, 1975), and corresponding to X_{BS} = 0.2. However, the radially averaged basalt profiles of all models discussed above (including the reference case), which all have an initial and bulk X_{BS} of 0.2, predict that the upper mantle is depleted in basaltic components relative to pyrolite.

As we vary the initial X_{BS} in this suite (all other parameters are fixed at reference values), we find that the radially averaged basalt profiles are shifted as a whole towards higher basalt fractions (Fig. 8). Accordingly, the average upper-mantle X_{BS} is also shifted. Obviously, case F4 is not Earth-like, since its radially averaged X_{BS} in the asthenosphere (see dashed red line in the yellow box in Fig. 8) is quite a bit higher (i.e., X_{BS} = 0.26) than that of pyrolite (i.e., X_{BS} = 0.2). In turn, cases F2 and F3 display asthenospheric average compositions similar to pyrolite (X_{BS} = 0.18 and 0.22, respectively). In these cases, the bulk lower mantle is significantly shifted towards higher basalt contents than pyrolite (see dashed lines in the green box in Fig. 8). In addition, the MTZ and lowermost mantle (thermochemical piles) display significant basalt reservoirs. Due to the significant enhancement of mafic (SiO_2-rich) basalt in case F3, even the shallow lower mantle

485 (660-1500 km depth, green box in Fig. 8) is mostly silicate perovskitic (bridgmanitic) on average
486 with a molar Mg/Si-ratio of 1.08 (i.e., calculated based on Table 1 in Xu et al., 2008). At 1500
487 km depth, the average molar Mg/Si ratio is ~1.07 and ~1.00 in cases F2 and F3, respectively.
488 According to our models, if indeed significant reservoirs of basalt exist in the MTZ and lower
489 mantle, the composition of the bulk-silicate Earth may be shifted towards basalt relative to the
490 uppermost-mantle composition of pyrolite, being more similar to the starting compositions of
491 cases F2 or F3. Accordingly, our previous estimation of $0.3 < X_{BS} < 0.35$ in the MTZ may be a
492 lower bound. Along these lines, segregation of basalt from harzburgite can help to filter
493 heterogeneity in order to sustain large-scale mantle layering, even in the presence of whole-
494 mantle convection.

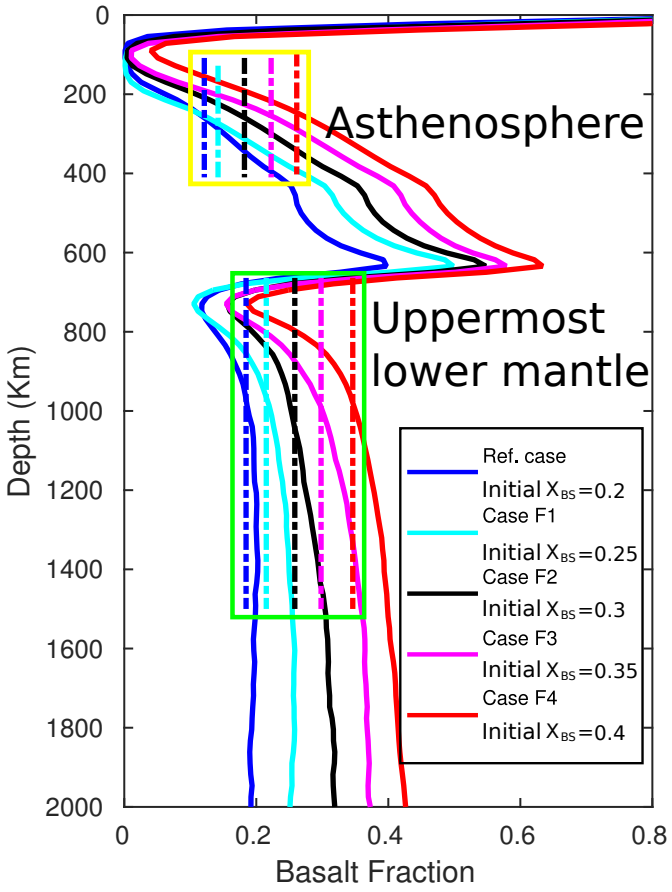

Fig. 8. Radial average X_{BS} (compositional index) between 2 and 4.5 Gyr for cases with different initial X_{BS}. Dashed lines in the yellow and green boxes denote average X_{BS} in the asthenosphere and uppermost lower mantle, respectively.

4. Discussion

One of the most striking and robust predictions of our models is that subducted basalt and harzburgite segregate from each other near the CMB, and that basalt ultimately accumulates in the MTZ and lower mantle. In turn, the asthenosphere and the layer just below 660 km depth are

504 relatively depleted in basaltic components compared to the mantle average. These predictions
505 result in systematic large-scale compositional layering on top of dominant small-scale and
506 regional-scale variations, consistent with previous global-scale mantle-convection models that
507 apply realistic density profiles for basalt and harzburgite (Ballmer et al., 2015; Nakagawa &
508 Buffett, 2005; Nakagawa et al., 2010). Our results are controlled by the well-constrained density
509 profiles of basalt and harzburgite (Fig. 1), and robust over a wide range of viscosity profiles (Fig.
510 S3). Moderate mantle layering is predicted to be sustained by segregation despite ongoing
511 whole-mantle convection and mixing, and to be soon established (within ~0.5 Gyr) after the
512 onset of basalt cycling. This cycling could be due to plate tectonics, or another mechanism such
513 as basalt dripping (Armann & Tackley, 2012), as likely relevant in the Archean (e.g., Fischer &
514 Gerya, 2016, Johnson et al., 2014). In case mafic crust enters the mantle as a hybrid lithology
515 such as pyroxenite (Bodinier & Godard, 2003; Castro & Gerya, 2008), the relevant density
516 profile and hence the style of segregation and mixing are expected to differ from that modeled
517 here.

518 As shown in section 3.4, this conclusion of moderate mantle layering implies that the
519 composition of the bulk-silicate Earth (BSE) is shifted relative to upper(most)-mantle pyrolite.
520 Indeed, such a difference in composition between the upper and lower mantles has been
521 proposed based on comparison of geophysical constraints with mineral-physics estimates of

lower-mantle rock properties (e.g., Murakami et al., 2012). Moreover, recent sound-velocity measurements of $CaSiO_3$ perovskite (Gréaux et al., 2019) imply an enrichment of basaltic crust in the Earth's lower mantle.

An enhancement of the BSE in basaltic materials further implies an enrichment in SiO_2, as well as in Al_2O_3 and CaO, relative to pyrolite. Thus, our models can reconcile the high Mg/Si ratio of pyrolite with the compositional range of chondrites (Ballmer et al., 2015). Our models also imply superchondritic Earth Al/Si and Ca/Si (e.g., McDonough & Sun, 1995). Al/Si and Ca/Si would have to be less superchondritic for E-chondrite than the CI-chondrite Earth building blocks (Javoy et al., 2010), or if mafic materials stored in the lower mantle are largely ancient (e.g., Archean basalt, komatiite), and hence depleted in Al+Ca relative to modern MORB (Hofmann & White, 1982; Arndt et al., 2008). In any case, our results point to some degree of fractionation of Al+Ca from Si+Mg during Earth accretion, which has been proposed to be due to a difference in condensation temperatures between Al+Ca and Si+Mg (Hart & Zindler, 1986; Lodders, 2003).

In our models, the dynamic mechanisms for the transport of mantle materials to the MTZ are slabs, and most importantly, plumes. We find that the relevant processes, such as entrainment of basaltic materials by plumes in the deep mantle, failure of plumes to carry these materials across the MTZ (Nakagawa & Buffett, 2005) and slab stagnation, depend on the mantle viscosity

structure. Moreover, the prerequisite for any delivery of basaltic material to (and accumulation in) any mantle reservoir, i.e., the segregation of basalt from harzburgite, also depends on the viscosity structure of the mantle. Segregation is more efficient for larger scale-lengths of heterogeneity, and for lower viscosities (Karato, 1997), but should be efficient as long as mantle viscosity is sufficiently small in at least some regions of the mantle. Indeed, very low viscosities are locally promoted, e.g. in the hot thermal boundary layer, or post-perovskite stability field (Ammann et al., 2010). Despite these large effects of mantle rheology, our models predict the degree of enrichment of basalt in the MTZ to be rather robust (about $0.3< X_{BS} <0.35$) over a wide range of viscosity profiles (see also section 3.2), mostly due to a universal balance between delivery/removal and reservoir capacity. This is an encouraging result given that the radial mantle viscosity profile remains poorly constrained (Rudolph et al., 2015). Due to this control by MTZ capacity, we also do not expect that model simplifications (such as 2-D geometry) affect the final compositional profile significantly. Note that 2-D models artificially increase efficiency of basalt delivery to MTZ by implying sheet-like plumes, but they also display artificially poor segregation near the CMB (Tackley, 2011). Indeed, previous 3-D models predict compositional stratification across the MTZ (Figure 5 in Nakagawa et al., 2010), although high-resolution studies are needed for further quantitative investigation.

556 It has been suggested that some hotspots are sourced by plumes that originate from the MTZ
557 (e.g., Mazza et al., 2019), while others are sourced by plumes that rise from the CMB, e.g. from
558 the margins of thermochemical piles (e.g., Burke et al., 2008). However, it remains unclear how
559 basalt can be transported from the MTZ reservoir to the surface. A possible explanation involves
560 that sub-lithospheric small-scale convection (Korenaga and Jordan, 2004) entrains a certain
561 amount of basalt from the MTZ reservoir. Alternatively, small-scale convection in, or hydrous
562 upwellings from, the MTZ may be relevant for the segregation of basalt in the MTZ (Long et al.,
563 2019; Motoki and Ballmer, 2015). In our global-scale geodynamic models, such rather small-
564 scale processes of convection and compositional segregation remain under-resolved due to
565 computational limitations (low spatial resolution). Therefore, the compositional layering
566 predicted here remains conservative.

567 Our robust model prediction of a basalt-reservoir in the MTZ, and a complementary harzburgite-
568 reservoir just below, can be tested using seismic data. A long-standing discussion involves
569 whether seismic properties of the MTZ can either be explained by a homogeneous pyrolite model
570 (Weidner, 1985) or by a basalt-enriched model (Agee, 1993). An accumulation of harzburgite
571 just below the MTZ can account for narrow high-velocity anomalies just beneath the MTZ in
572 regions of mantle upwelling (Maguire et al., 2017). Based on a joint seismological and mineral-
573 physics analysis, Yu et al. (2018) present direct evidence for local harzburgite enrichment near

574 the base of the MTZ beneath Hawaii. More recently, Wu et al. (2019) suggest chemical layering
575 in regions with short-scale topography of the 660-km discontinuity. Note that our models also
576 predict that a global reservoir can be maintained, at least for cases with relatively low reference
577 viscosity, even though both slabs and plumes can destroy the formed basalt-
578 enriched/harzburgite-enriched reservoir locally. However, more geophysical observations are
579 needed to confirm the nature of regional, or even global, reservoirs near 660 km depth.

580 **5. Conclusion**

581 Our global-scale thermo-chemical convection models show that deep-rooted plumes (and to a
582 minor extent, stagnant slabs) play an important role in terms of delivering basalt/harzburgite to
583 the layers at the base/just below the MTZ, and to establish a laterally variable basalt-
584 /harzburgite-enriched reservoir. The amount of basalt accumulated in the MTZ does not depend
585 very much on the mantle viscosity structure, which is the result of a balance between delivery,
586 removal and capacity of the MTZ. In turn, the amount of basalt accumulated above the CMB
587 strongly depends on mantle viscosity structure. Our models predict that regional reservoirs in the
588 MTZ are moderately-to-strongly enhanced by basalt (12%~37% on average) relative to pyrolite
589 (i.e., compositional index 0.3~0.5), while most regional harzburgite-enriched reservoirs beneath
590 the MTZ are enhanced by 40%~80% (compositional index 0.04~0.12). This prediction is

consistent with estimates from seismology, although more regional or even global studies are needed for further confirmation. The resulting compositional mantle layering is typically associated with a subadiabatic potential-temperature gradient across the MTZ. Finally, the composition of the bulk-silicate Earth may be shifted relative to that of the upper-mantle pyrolite if indeed significant reservoirs of basalt exist in the MTZ and lower mantle. Our results suggest that the segregation of basalt from harzburgite can act to filter mantle heterogeneity in order to sustain a layering mantle composition. The mantle flow that is related to sustaining the basalt-enriched MTZ (and harzburgite-enriched) reservoir may play an important role in regulating heat and material fluxes through the mantle.

Acknowledgments

J.Y. was funded by the Chinese Government Scholarship. P.T. acknowledges support from the Swiss Platform for Advanced Scientific Computing (StagBL project).

References

Agee, C. B. (1993). Petrology of the mantle transition zone. Annual Review of Earth and Planetary Sciences, 21(1), 19-41.

Allègre, C. J., & Turcotte, D. L. (1985). Geodynamic mixing in the mesosphere boundary layer and the origin of oceanic islands. Geophysical Research Letters, 12(4), 207-210.

608 Ammann, M.W., Brodholt, J.P., Wookey, J., Dobson, D.P., 2010. First-principles constraints on
609 diffusion in lower-mantle minerals and a weak D layer. Nature 465(7297), 462–465.

610 Anderson, D. L. (1979). Chemical stratification of the mantle. Journal of Geophysical Research:
611 Solid Earth, 84(B11), 6297-6298.

612 Armann, M., & Tackley, P. J. (2012). Simulating the thermochemical magmatic and tectonic
613 evolution of Venus's mantle and lithosphere: Two-dimensional models. Journal of Geophysical
614 Research: Planets, 117(E12).

615 Arndt, N.T., Lesher, C.M., & Barnes, S.J. (2008). Komatiite. Cambridge University Press,
616 Cambridge. 467 pp.

617 Ballmer, M. D., Houser, C., Hernlund, J. W., Wentzcovitch, R. M., & Hirose, K. (2017).
618 Persistence of strong silica-enriched domains in the Earth's lower mantle. Nature
619 Geoscience, 10(3), 236.

620 Ballmer, M. D., Schmerr, N. C., Nakagawa, T., & Ritsema, J. (2015). Compositional mantle
621 layering revealed by slab stagnation at ~1000-km depth. Science advances, 1(11), e1500815.

622 Ballmer, M. D., Schumacher, L., Lekic, V., Thomas, C. & Ito, G (2016). Compositional layering
623 within the large low shear-wave velocity provinces in the lower mantle. Geochemistry,
624 Geophysics, Geosystems, 17, 5056-5077.

625 Bentham, H. L. M., & Rost, S. (2014). Scattering beneath Western Pacific subduction zones:
626 evidence for oceanic crust in the mid-mantle. Geophysical Journal International, 197(3), 1627-
627 1641.

628 Bodinier, J. L., & Godard, M. (2003). Orogenic, ophiolitic, and abyssal peridotites. Treatise on
629 geochemistry, 2, 568.

630 Brandenburg, J. P., & Van Keken, P. E. (2007). Deep storage of oceanic crust in a vigorously
631 convecting mantle. Journal of Geophysical Research: Solid Earth, 112(B6).

632 Burke, K., Steinberger, B., Torsvik, T. H., & Smethurst, M. A. (2008). Plume generation zones
633 at the margins of large low shear velocity provinces on the core–mantle boundary. Earth and
634 Planetary Science Letters, 265(1-2), 49-60.

635 Castro, A., & Gerya, T. V. (2008). Magmatic implications of mantle wedge plumes:
636 experimental study. Lithos, 103(1-2), 138-148.

637 Christensen, U. R., & Hofmann, A. W. (1994). Segregation of subducted oceanic crust in the
638 convecting mantle. Journal of Geophysical Research: Solid Earth, 99(B10), 19867-19884.

639 Davies, G. F. (2008). Episodic layering of the early mantle by the 'basalt barrier'
640 mechanism. Earth and Planetary Science Letters, 275(3-4), 382-392.

641 Dziewonski, A. M., Lekic, V., & Romanowicz, B. A. (2010). Mantle anchor structure: an
642 argument for bottom up tectonics. Earth and Planetary Science Letters, 299(1-2), 69-79.

643 Fischer, R., & Gerya, T. (2016). Early Earth plume-lid tectonics: A high-resolution 3D numerical
644 modelling approach. Journal of Geodynamics, 100, 198-214.

645 Garnero, E. J., McNamara, A. K., & Shim, S. H. (2016). Continent-sized anomalous zones with
646 low seismic velocity at the base of Earth's mantle. Nature Geoscience, 9(7), 481.

647 Gréaux, S., Irifune, T., Higo, Y., Tange, Y., Arimoto, T., Liu, Z., & Yamada, A. (2019). Sound
648 velocity of CaSiO 3 perovskite suggests the presence of basaltic crust in the Earth's lower
649 mantle. Nature, 565(7738), 218.

650 Hart, S. R., & Zindler, A. (1986). In search of a bulk-Earth composition. Chemical
651 Geology, 57(3-4), 247-267.

652 Hirose, K., Fei, Y., Ma, Y., & Mao, H. K. (1999). The fate of subducted basaltic crust in the
653 Earth's lower mantle. Nature, 397(6714), 53.

654 Hofmann, A. W. (1997). Mantle geochemistry: the message from oceanic volcanism. Nature,
655 385(6613), 219.

656 Hofmann, A. W., & White, W. M. (1982). Mantle plumes from ancient oceanic crust. Earth and
657 Planetary Science Letters, 57(2), 421-436.

Irifune, T., & Ringwood, A. E. (1993). Phase transformations in subducted oceanic crust and buoyancy relationships at depths of 600–800 km in the mantle. Earth and Planetary Science Letters, 117(1-2), 101-110.

Ishii, M., & Tromp, J. (1999). Normal-mode and free-air gravity constraints on lateral variations in velocity and density of Earth's mantle. Science, 285(5431), 1231-1236.

Javoy, M., Kaminski, E., Guyot, F., Andrault, D., Sanloup, C., Moreira, M., ... & Jaupart, C. (2010). The chemical composition of the Earth: Enstatite chondrite models. Earth and Planetary Science Letters, 293(3-4), 259-268.

Johnson, T. E., Brown, M., Kaus, B. J., & VanTongeren, J. A. (2014). Delamination and recycling of Archaean crust caused by gravitational instabilities. Nature Geoscience, 7(1), 47.

Kaneshima, S., & Helffrich, G. (1999). Dipping low-velocity layer in the mid-lower mantle: evidence for geochemical heterogeneity. Science, 283(5409), 1888-1892.

Karato, S. I. (1997). On the separation of crustal component from subducted oceanic lithosphere near the 660 km discontinuity. Physics of the Earth and Planetary Interiors, 99(1-2), 103-111.

Koelemeijer, P., Ritsema, J., Deuss, A., & Van Heijst, H. J. (2015). SP12RTS: a degree-12 model of shear-and compressional-wave velocity for Earth's mantle. Geophysical Journal International, 204(2), 1024-1039.

675 Korenaga, J., & Jordan, T. H. (2004). Physics of multiscale convection in Earth's mantle:
676 Evolution of sublithospheric convection. Journal of Geophysical Research: Solid Earth, 109(B1).
677 Lee, C. T. A., & Chen, W. P. (2007). Possible density segregation of subducted oceanic
678 lithosphere along a weak serpentinite layer and implications for compositional stratification of
679 the Earth's mantle. Earth and Planetary Science Letters, 255(3-4), 357-366.
680 Lodders, K. (2003). Solar system abundances and condensation temperatures of the
681 elements. The Astrophysical Journal, 591(2), 1220.
682 Long, X., Ballmer, M. D., Córdoba, A. M. C., & Li, C. F. (2019). Mantle melting and intraplate
683 volcanism due to self-buoyant hydrous upwellings from the stagnant slab that are conveyed by
684 small-scale convection. Geochemistry, Geophysics, Geosystems.
685 Maguire, R., Ritsema, J., & Goes, S. (2017). Signals of 660 km topography and harzburgite
686 enrichment in seismic images of whole- mantle upwellings. Geophysical Research Letters, 44(8),
687 3600-3607.
688 Mazza, S. E., Gazel, E., Bizimis, M., Moucha, R., Béguelin, P., Johnson, E. A., ... & Sobolev, A.
689 V. (2019). Sampling the volatile-rich transition zone beneath Bermuda. Nature, 569(7756), 398.
690 McDonough, W. F., & Sun, S. S. (1995). The composition of the Earth. Chemical
691 geology, 120(3-4), 223-253.

692 Motoki, M. H., & Ballmer, M. D. (2015). Intraplate volcanism due to convective instability of
693 stagnant slabs in the mantle transition zone. Geochemistry, Geophysics, Geosystems, 16(2), 538-
694 551.

695 Mukhopadhyay, S. (2012). Early differentiation and volatile accretion recorded in deep-mantle
696 neon and xenon. Nature, 486(7401), 101.

697 Mulyukova, E., Steinberger, B., Dabrowski, M., & Sobolev, S. V. (2015). Survival of LLSVPs
698 for billions of years in a vigorously convecting mantle: replenishment and destruction of
699 chemical anomaly. Journal of Geophysical Research: Solid Earth, 120(5), 3824-3847.

700 Mundl, A., Touboul, M., Jackson, M. G., Day, J. M., Kurz, M. D., Lekic, V., & Walker, R. J.
701 (2017). Tungsten-182 heterogeneity in modern ocean island basalts. Science, 356(6333), 66-69.

702 Murakami, M., Y. Ohishi, N. Hirao, and K. Hirose (2012), A perovskitic lower mantle inferred
703 from high-pressure, high-temperature sound velocity data, Nature, 485(7396), 90–U118.

704 Nakagawa, T., & Buffett, B. A. (2005). Mass transport mechanism between the upper and lower
705 mantle in numerical simulations of thermochemical mantle convection with multicomponent
706 phase changes. Earth and Planetary Science Letters, 230(1-2), 11-27.

707 Nakagawa, T., & Tackley, P. J. (2005). The interaction between the post-perovskite phase
708 change and a thermo-chemical boundary layer near the core–mantle boundary. Earth and
709 Planetary Science Letters, 238(1-2), 204-216.

710 Nakagawa, T., & Tackley, P. J. (2010). Influence of initial CMB temperature and other
711 parameters on the thermal evolution of Earth's core resulting from thermochemical spherical
712 mantle convection. Geochemistry, Geophysics, Geosystems, 11(6).

713 Nakagawa, T., & Tackley, P. J. (2012). Influence of magmatism on mantle cooling, surface heat
714 flow and Urey ratio. Earth and Planetary Science Letters, 329, 1-10.

715 Nakagawa, T., & Tackley, P. J. (2015). Influence of plate tectonic mode on the coupled
716 thermochemical evolution of Earth's mantle and core. Geochemistry, Geophysics,
717 Geosystems, 16(10), 3400-3413.

718 Nakagawa, T., Tackley, P. J., Deschamps, F., & Connolly, J. A. (2010). The influence of MORB
719 and harzburgite composition on thermo-chemical mantle convection in a 3-D spherical shell with
720 self-consistently calculated mineral physics. Earth and Planetary Science Letters, 296(3-4), 403-
721 412.

722 Ogawa, M. (2000). Numerical models of magmatism in convecting mantle with temperature-
723 dependent viscosity and their implications for Venus and Earth. Journal of Geophysical
724 Research: Planets, 105(E3), 6997-7012.

725 Ringwood, A. E. (1975). Composition and Petrology of the Earth's Mantle. McGraw-Hill, New
726 York.

727 Ringwood, A. E., & Irifune, T. (1988). Nature of the 650–km seismic discontinuity: implications
728 for mantle dynamics and differentiation. Nature, 331(6152), 131.

729 Rizo, H., Boyet, M., Blichert-Toft, J., & Rosing, M. T. (2013). Early mantle dynamics inferred
730 from 142Nd variations in Archean rocks from southwest Greenland. Earth and Planetary Science
731 Letters, 377, 324-335.

732 Rost, S., Garnero, E. J., & Williams, Q. (2008). Seismic array detection of subducted oceanic
733 crust in the lower mantle. Journal of Geophysical Research: Solid Earth, 113(B6).

734 Rudolph, M. L., Lekić, V., & Lithgow-Bertelloni, C. (2015). Viscosity jump in Earth's mid-
735 mantle. Science, 350(6266), 1349-1352.

736 Sinha, G., & Butler, S. L. (2007). On the origin and significance of subadiabatic temperature
737 gradients in the mantle. Journal of Geophysical Research: Solid Earth, 112(B10).

738 Stixrude, L., & Lithgow-Bertelloni, C. (2012). Geophysics of chemical heterogeneity in the
739 mantle. Annual Review of Earth and Planetary Sciences, 40, 569-595.

740 Tackley, P. J. (2008). Modelling compressible mantle convection with large viscosity contrasts
741 in a three-dimensional spherical shell using the yin-yang grid. Physics of the Earth and Planetary
742 Interiors, 171(1-4), 7-18.

743 Tackley, P. J. (2011). Living dead slabs in 3-D: The dynamics of compositionally-stratified slabs
744 entering a “slab graveyard” above the core-mantle boundary. Physics of the Earth and Planetary
745 Interiors, 188(3-4), 150-162.

746 Tackley, P. J. (2012). Dynamics and evolution of the deep mantle resulting from thermal,
747 chemical, phase and melting effects. Earth-Science Reviews, 110(1-4), 1-25.

748 van Keken, P. E., Karato, S., & Yuen, D. A. (1996). Rheological control of oceanic crust
749 separation in the transition zone. Geophysical Research Letters, 23(14), 1821-1824.

750 Waszek, L., Schmerr, N. C., & Ballmer, M. D. (2018). Global observations of reflectors in the
751 mid-mantle with implications for mantle structure and dynamics. Nature communications, 9(1),
752 385.

753 Weidner, D. J. (1985). A mineral physics test of a pyrolite mantle. Geophysical Research Letters,
754 12(7), 417-420.

Wu, W., Ni, S., & Irving, J. C. (2019). Inferring Earth's discontinuous chemical layering from the 660-kilometer boundary topography. Science, 363(6428), 736-740.

Xu, W., Lithgow-Bertelloni, C., Stixrude, L., & Ritsema, J. (2008). The effect of bulk composition and temperature on mantle seismic structure. Earth and Planetary Science Letters, 275(1-2), 70-79.

Yu, C., Day, E. A., Maarten, V., Campillo, M., Goes, S., Blythe, R. A., & van der Hilst, R. D. (2018). Compositional heterogeneity near the base of the mantle transition zone beneath Hawaii. Nature communications, 9(1), 1266.